AGU PUBLICATIONS

Geophysical Research Letters

RESEARCH LETTER
10.1002/2016GL069405

Key Points:
- Helmholtz decomposition of second-order structure functions using Lagrangian observations from the Gulf of Mexico is presented
- Divergent motions dominate below 5 km, while rotational components dominate at larger scales
- Third-order velocity structure function indicates a forward energy cascade acting at scales below 2 km

Supporting Information:
- Supporting Information S1

Correspondence to:
D. Balwada,
db10d@fsu.edu

Citation:
Balwada, D., J. H. LaCasce, and K. G. Speer (2016), Scale-dependent distribution of kinetic energy from surface drifters in the Gulf of Mexico, *Geophys. Res. Lett.*, *43*, 10,856–10,863, doi:10.1002/2016GL069405.

Received 29 APR 2016
Accepted 12 SEP 2016
Accepted article online 16 SEP 2016
Published online 19 OCT 2016

Scale-dependent distribution of kinetic energy from surface drifters in the Gulf of Mexico

Dhruv Balwada[1], Joseph H. LaCasce[2], and Kevin G. Speer[1,3]

[1]Geophysical Fluid Dynamics Institute, Florida State University, Tallahassee, Florida, USA, [2]Department of Geosciences, University of Oslo, Oslo, Norway, [3]Department of Earth, Ocean and Atmospheric Science, Florida State University, Tallahassee, Florida, USA

Abstract The scale-dependent distribution of kinetic energy is probed at the surface in the Gulf of Mexico using surface drifters from the Grand Lagrangian Deployment (GLAD) experiment. The second-order velocity structure function and its decomposition into rotational and divergent components are examined. The results reveal that the divergent component, compared to the rotational component, dominates at scales below 5 km, and the pattern is reversed at larger scales. The divergent component has a slope near 2/3 below 5 km, similar to an energy cascade range ($k^{-5/3}$). The third-order velocity structure function at scales below 5 km is negative and implies a forward cascade of energy to smaller scales. The rotational component has a steeper slope, roughly 1.5, from scales of 5 km up to the deformation radius. This is similar to a 2-D enstrophy cascade, although the slope is shallower than the predicted 2. There is a brief 2/3 range from the deformation radius to 200 km, suggestive of a 2-D inverse cascade.

1. Introduction

Macroscopic turbulence in the atmosphere and the ocean is responsible for the fluxes of energy, enstrophy, and tracer variance across scales. Knowing the nature of turbulence that is occurring indicates, for example, whether the energy is cascading toward larger or smaller scales. In the upper troposphere, the kinetic energy spectrum was calculated with startling clarity from velocity measurements via commercial aircraft [*Gage and Nastrom*, 1986]. The results suggested a 2-D turbulent cascade (of enstrophy) [*Kraichnan*, 1967; *Charney*, 1971] from the baroclinic deformation radius, of order 2000 km in the atmosphere, down to several hundred kilometers. The kinetic energy spectrum was shallower at smaller scales, exhibiting the $k^{-5/3}$ slope expected for a turbulent energy cascade, where k is the polar wave number. The nature of this latter range has been attributed to inertia-gravity waves [*Callies et al.*, 2014], stratified turbulence [*Lindborg*, 2006, 2015], and surface dynamics [*Tulloch and Smith*, 2006] and remains a subject of debate.

The ocean is more challenging in this regard, measuring the kinetic energy spectrum, because the deformation radius is smaller, typically 10–50 km [*Chelton et al.*, 1998]. Thus, gridded satellite data, with a typical resolution of 100 km, are unable to resolve subdeformation scales [*Stammer*, 1997]. Continuous shipboard current measurements using acoustic techniques (acoustic Doppler current profiler, ADCP) have better resolution (∼1–5 km). Studies using these ADCP data have given indications of an enstrophy range, as in the atmosphere, at length scales approximately between 30 and 100 km in different parts of the ocean [*Wang et al.*, 2009; *Callies and Ferrari*, 2013; *Bühler et al.*, 2014; *Rocha et al.*, 2015], with some minor regional differences in scales. However, these analyses have also revealed that the dynamics between 5 and 30 km have a significant contribution from ageostrophic flows and differ from predictions of traditional quasi-geostrophic dynamics. It should be noted, even using ADCP data, that the length scales (<5 km) where the Rossby number is order 1, are barely resolved.

GPS-tracked surface drifters, on the other hand, can resolve horizontal scales down to 10 m, in principle, 2 orders of magnitude finer than with shipboard ADCP. The present work builds on previous studies, which quantified the nature of the energy spectrum in the ocean, by using surface drifter data. A convenient diagnostic for use with drifter data is the second-order velocity structure function ($D2$ hereafter), which is related to the energy spectrum and can be decomposed into rotational and divergent parts [*Bühler et al.*, 2014; *Callies et al.*, 2014; *Lindborg*, 2015]. We also examine higher-order velocity structure functions to characterize other aspects of the turbulent behavior.

2. Methods

Structure functions are calculated from the velocities of pairs of drifters. We define the longitudinal velocity, the component along the separation vector $\mathbf{r} = \Delta x\hat{i} + \Delta y\hat{j}$, $\Delta x = (x_2 - x_1)$ and $\Delta y = (y_2 - y_1)$, are the zonal and meridional components), as $\mathbf{u_l} = \frac{\mathbf{r}.\mathbf{u}}{|\mathbf{r}|}\hat{l}$ and the transverse velocity as $\mathbf{u_t} = \frac{(\mathbf{r}\times\mathbf{u}).\hat{\mathbf{k}}}{|\mathbf{r}|}\hat{t}$ ($\hat{l}$ and $\hat{t}$ are unit vectors in the longitudinal and transverse directions, respectively). The velocity difference between the drifters can be similarly projected.

Any velocity vector ($\mathbf{u}$) can be expressed as a sum of a rotational ($\mathbf{u_r}$) and a divergent ($\mathbf{u_d}$) component:

$$\mathbf{u} = \mathbf{u_r} + \mathbf{u_d} = -\nabla \times (\mathbf{k}\psi) + \nabla\phi, \tag{1}$$

where ∇ is the horizontal gradient operator, $\mathbf{k}$ is the vertical unit vector, ψ the stream function, and ϕ the velocity potential [*Bühler et al.*, 2014]. This (Helmholtz) decomposition is nonunique. However, assuming doubly periodic boundary conditions the stream function might differ at most by a constant, which does not affect the velocities.

The velocity structure functions are the moments of the velocity difference between the two drifters, $\delta\mathbf{u}$. $D2$, the mean of the squared difference, for homogeneous and isotropic flows is related to the kinetic energy spectrum via the Fourier transform [*Bennett*, 1984] and can be shown to be

$$D2(r) = 2\int_0^\infty E(k)(1 - J_0(kr))\mathrm{d}k, \tag{2}$$

where $E(k)$ is the energy spectrum, $J_0(kr)$ is the zeroth-order Bessel function, r is the separation, and k is the polar wave number. Using the asymptotic limits of $(1 - J_0(kr))$,

$$\frac{1}{2}D2(r) \approx \frac{r^2}{4}\int_0^{2/r} k^2E(k)dk + \int_{2/r}^\infty E(k)\mathrm{d}k. \tag{3}$$

This relationship reveals the physical significance of $D2$ and its relation to the spectrum. The $D2(r)$ is a cumulative quantity that sums the energy of eddies that are smaller than $\pi r/2$ and the enstrophy of the eddies that are larger than $\pi r/2$, where the length scale corresponding to wave number k is pi/k. This can be physically understood as the eddies that are smaller than the separation distance contribute their kinetic energy to the $D2$, while the eddies that are larger than separation distance contribute through their imposed velocity gradient to $D2$ [*Davidson and Pearson*, 2005; *Davidson*, 2015].

$D2(r)$ also can be separated into components, $D2_l = \delta u_l^2$ and $D2_t = \delta u_t^2$. Scaling arguments, such as those applied for the kinetic energy spectrum in the turbulent inertial ranges, apply here as well: $D2_t \sim D2_l \sim r^m$ if $E_l \sim E_t \sim k^{-(m+1)}$, provided that $m + 1 \leq 3$ [e.g., *Babiano et al.*, 1985; *Bennett*, 1984; *Lindborg*, 2007]. Also, the length scale where different components of $D2(r)$ intersect, indicating the length scale where the different flow components (longitudinal and transverse or rotational and divergent) exchange dominance, provides a reasonable approximation to the length scale where the corresponding components of $E(k)$ intersect for the results presented in this study. This is discussed further in the supporting information.

Under certain conditions, the transverse and longitudinal structure functions are related [*Lindborg*, 2007]. For purely rotational 2-D flow (horizontally nondivergent), the incompressibility condition yields

$$D2_t = \frac{\mathrm{d}}{\mathrm{d}r}(rD2_l). \tag{4}$$

For potential flow (horizontally irrotational), the condition of zero curl yields

$$D2_l = \frac{\mathrm{d}}{\mathrm{d}r}(rD2_t). \tag{5}$$

Thus, if the second-order velocity structure function exhibits a power law dependence, $D2_t \sim D2_l \sim r^m$, the above relations imply the ratio $D2_t/D2_l = m + 1$ for a purely rotational flow and $D2_l/D2_t = m + 1$ for a purely divergent flow [*Lindborg*, 1999; *Bühler et al.*, 2014].

If the rotational and divergent components are uncorrelated, the second-order velocity structure function is simply their sum [*Lindborg*, 2015]. This equals the sum of the functions based on the rotational and divergent velocities as well, as

$$D2 = D2_l + D2_t = D2_r + D2_d. \tag{6}$$

Under the assumptions of homogeneity, isotropy, and the uncorrelated components, the following expressions are obtained:

$$D2_r = D2_t + \int_0^r \frac{1}{r}(D2_t - D2_l)\mathrm{d}r, \tag{7}$$

and

$$D2_d = D2_l - \int_0^r \frac{1}{r}(D2_t - D2_l)\mathrm{d}r. \tag{8}$$

Higher-order velocity structure functions can also be calculated, and these can reveal more about the turbulence. The third-order velocity structure function, defined $D3_l =< \delta u_l \delta\mathbf{u}.\delta\mathbf{u} >$, is related to the spectral energy or enstrophy flux [*Frisch*, 1995; *Lindborg and Cho*, 2001]. The sign in particular, if the $D3_l$ is linear, reflects the direction of energy transfer, either upscale or downscale. The fourth-order velocity structure function is often written as a kurtosis; e.g., $F_l = \frac{<\delta u_l^4>}{<\delta u_l^2>^2}$ for the longitudinal component. This indicates the degree of non-Gaussianity or intermittency as a function of scale.

3. Dynamical Expectations

Kolmogorov used velocity structure functions in developing his theory for 3-D turbulence at high Reynolds numbers [*Kolmogorov*, 1941; *Frisch*, 1995]. With a constant flux of energy across scales, ϵ, the second-order velocity structure function scales as $D2 \propto \epsilon^{2/3} r^{2/3}$, Kolmogorov's "2/3 law." The same dependence applies to an inverse energy cascade in 2-D turbulence. He also showed that the third-order longitudinal velocity structure function, $D3_l$, equals $-4/5\epsilon r$, an exact result (his "4/5 law"). The function equals $-2\epsilon r$ in a quasi-2-D forward energy range [*Lindborg and Cho*, 2001] and $2\epsilon r$ in the 2-D inverse energy range [*Lindborg*, 1999], where ϵ is a positive quantity and a positive/negative $D3_l$ indicates an upscale/downscale energy transfer. In a 2-D enstrophy cascade, the scaling is instead $D2 \propto \eta^{2/3} r^2$, where η is the enstrophy flux [e.g., *Lindborg*, 1999; *LaCasce*, 2002]. The third-order longitudinal function in this case equals to $1/4\eta r^3$ [*Lindborg*, 1999].

There are of course other possibilities at the ocean surface. Under surface quasi-geostrophy, there are also two inertial ranges, one for total energy and one for temperature variance [*Held et al.*, 1995]. There are claims that the latter occurs at the ocean surface [e.g., *Le Traon et al.*, 2008], but observational evidence is currently lacking [*Callies and Ferrari*, 2013; *Rocha et al.*, 2015]. The energy spectrum is the same as in an energy cascade and also yields an $r^{2/3}$ dependence for $D2$. A similar spectral slope is seen in the high wave number range of the empirical Garret and Munk spectrum, with energy cascading downscale due to wave-wave interactions [*Garrett and Munk*, 1972]. Other possibilities exist, due for example to frontal processes, inertial oscillations and Langmuir turbulence [*Thomas et al.*, 2008]. Thus, it is not clear a priori that a single scaling regime should apply.

4. Results

The trajectories of the GLAD drifters are shown in Figure 1. These lie in the northeastern Gulf of Mexico and span the period from July to October in 2012. The drifters were launched in clusters, with a minimum initial separation of 100 m [*Poje et al.*, 2014]. However, smaller separations or "chance pairs" [*Morel and Larceveque*, 1974; *LaCasce and Ohlmann*, 2003] also occurred.

The Lagrangian kinetic energy frequency spectrum, shown in the insert in Figure 1, has a typical shape: flat at low frequencies and decreasing as ω^{-2} at high [*Rupolo et al.*, 1996; *LaCasce*, 2008]. A significant inertial peak is also seen, clearly visible as anticyclonic loops in the trajectories.

The structure functions were averaged using distance bins with a size distribution given by $r_k = 0.1 \times 1.4^k$ m, yielding equal spacing on a logarithmic scale. The smallest bin, at 10 m separation, has more than 5000 velocity estimates, and there are more than 10^7 at 200 km. The nominal position and velocity errors are expected to be 10 m and 3 cm/s, respectively, which result from errors in GPS positioning along with interpolation and smoothing operations that are used to obtain the 15 min resolution. A detailed account of these position and velocity errors can be found in the metadata provided with the data set. Random errors on the second-order velocity structure functions are extremely small (Figure S1 in the supporting information) and thus provide us

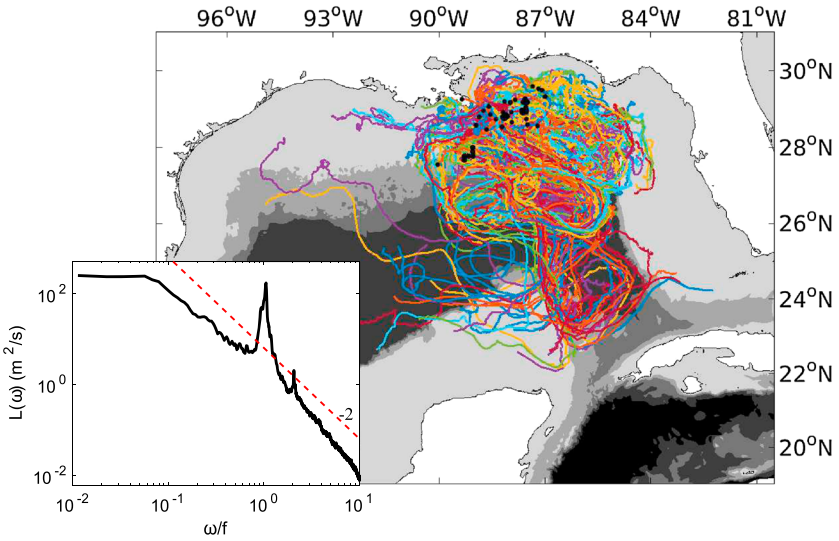

Figure 1. Surface drifter trajectories from Grand Lagrangian Deployment (GLAD) experiment conducted in 2012, where each colored line represents a single trajectory and the black dots represent the deployment locations. Contour shading represents bathymetry between 0 to 5000 m, contour intervals of 1000 m. Bottom left inset shows the averaged Lagrangian kinetic energy frequency spectrum of the velocity time series from these surface drifters. Dashed red line represents power law behavior of ω^{-2}.

confidence in the results. The random errors are greater for the third-order velocity structure function, as it is not an average of a sign definite quantity, but they do not obscure the key qualitative results presented here.

The longitudinal and transverse pair velocity correlations (not shown) suggest strongly correlated motion up to separations of 50 km, as noted previously by [*Beron-Vera and LaCasce*, 2016]. Pairs with separations exceeding 100 km display uncorrelated motion. $D2$ has a slope near 2/3 up to about 200 km (Figure 2a), also noted previously [*Poje et al.*, 2014; *Beron-Vera and LaCasce*, 2016]. At larger scales $D2$ flattens out, as the pair velocity correlation goes to zero ($D2 = <\delta \boldsymbol{u}^2> = 2 < |\mathbf{u}|^2 > -2 < \mathbf{u_1} \cdot \mathbf{u_2} >$).

The different components of $D2$ are also shown in Figure 2a. Most conspicuously, the rotational and divergent components cross at roughly 5 km separation, with the divergent component dominating at smaller scales and the rotational component at larger. Likewise, the transverse and longitudinal velocity structure functions cross near this scale, with the transverse component dominating at large scales and the longitudinal component being somewhat larger at small scales. The Rossby number can be estimated as $Ro = \sqrt{D2_l + D2_t}/(fr)$,

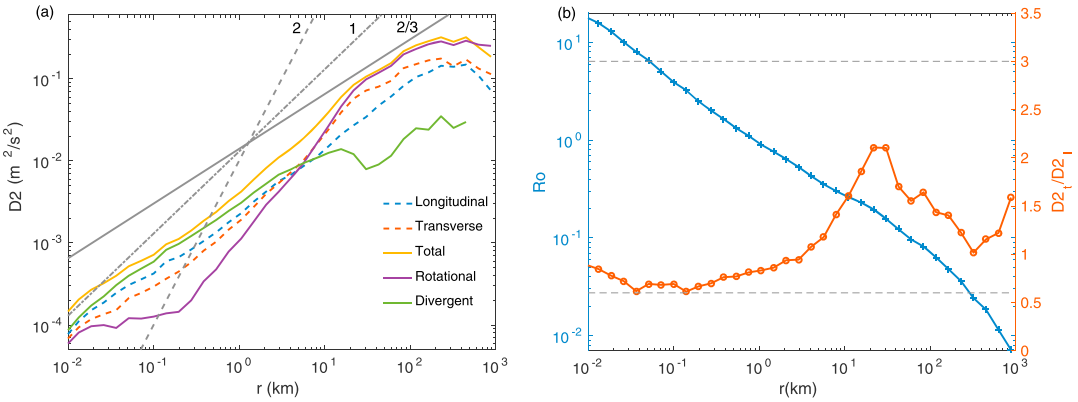

Figure 2. (a) Different components of the second-order velocity structure functions. Three power law relationships are plotted as gray lines with slopes marked on the top. (b) Left axis, blue, shows the Rossby number defined as $\sqrt{D2}/(fr)$, where f is the Coriolis parameter and r is the separation distance. Right axis, orange, shows the ratio of the transverse to longitudinal second-order velocity structure function ($D2_t/D2_l$).

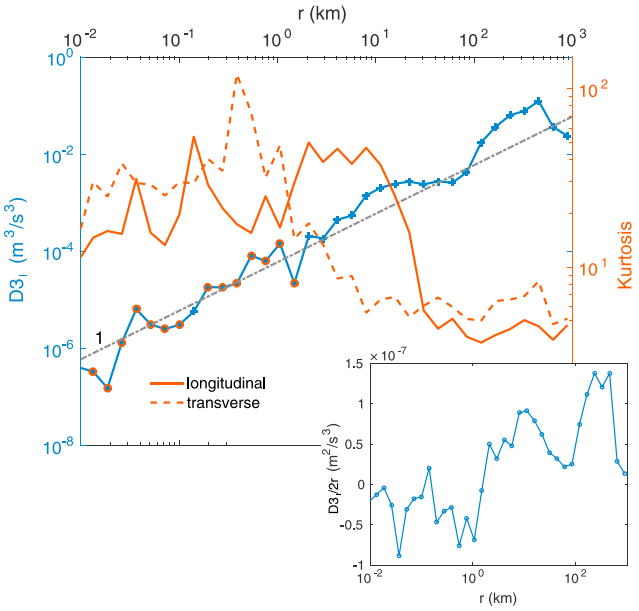

Figure 3. Absolute value of the longitudinal component of the third-order velocity structure function ($D3_l$) on the left axis (blue axis and line). Orange circles and blue pluses represent negative and positive values, respectively. A linear power law relationship is shown as dashed gray line. Kurtosis ($\frac{<\delta u^4>}{<\delta u^2>^2}$), both longitudinal and transverse components, is shown in orange on the right axis. Inset on bottom right shows the relation $D3_l/2r$.

where f is the Coriolis parameter and r the separation. The transition scale is approximately where the Ro is unity (Figure 2b). Ro is smaller at larger scales, indicating the flow is nearer to geostrophic balance and hence rotational [*Pedlosky*, 1987].

At small scales, the divergent velocity structure function, $D2_d$, has a slope near 2/3, as expected for an energy range. This essentially determines the slope of the total function, $D2$. Further, the ratio of the transverse and longitudinal velocity structure functions is close to 3/5 (Figure 2b), as expected for a divergent flow with a slope of 2/3.

From 5 to 50 km, the rotational velocity structure function is greater. Below roughly 30 km, this has a slope of 1.5. The steeper $D2_r$ accounts for the steepening in $D2$ seen above 5 km. The deformation radius, L_d, in the Gulf of Mexico is near 45 km [*Chelton et al.*, 1998], so the rotational velocity structure function resembles that for an enstrophy cascade below L_d but has a shallower slope than 2. The ratio $D2_t/D2_l$ increases rapidly in the range of 5–50 km to a value of 2.2 (the theoretical value for an enstrophy cascade is 3 with a slope of 2 for the velocity structure function).

Between 40 and 100 km, $D2$ essentially reflects $D2_r$. The slope in this range is near 2/3, suggestive of a 2-D inverse energy cascade. However, the range of scales is small. The ratio $D2_t/D2_l$ is falling but is obviously not constant (Figure 2b).

The higher-order moments provide additional insight. The longitudinal third-order velocity structure function, $D3_l$, increases approximately linearly over all scales below 200 km (Figure 3). A linear slope is expected in an energy cascade (section 3). $D3_l$ is positive at the larger scales but changes sign at 2 km. The negative, linear dependence at small scales implies a forward energy cascade. A similar result was obtained previously with atmospheric data, below 100 km, by *Cho and Lindborg* [2001]. The implied dissipation rate, $\epsilon = D3_l/(2r)$ with the sign signifying the direction, is shown in the insert in Figure (3). Below 2 km the value is approximately 5×10^{-8} m^2/s^3 and negative, which is in line with estimates of energy dissipation rate based on microstructure measurements in the near surface ocean [*Moum and Smyth*, 2001].

The positive, linear $D3_l$, seen here at the larger scales, would imply an upscale transfer in an energy cascade. However, as the divergent and rotational components are both present in the range of 2–20 km, the result probably represents a combination of the positive, cubic behavior expected in an enstrophy range (section 3) with the negative contribution from the divergent motions.

The longitudinal and transverse kurtoses are shown in orange in Figure (3). The two are consistent in that the small scales are non-Gaussian while the scales above L_d are nearer Gaussian. However, the transition scale differs slightly for the two, occurring near 5 km for the transverse function and 20 km for the longitudinal. The kurtosis is expected to be non-Gaussian in either an energy or enstrophy range and Gaussian at scales where the pair motion is uncorrelated.

Homogeneity and isotropy are essential for the turbulence scaling laws and the Helmholtz decomposition to hold. However, these assumptions are rarely, if ever, perfectly satisfied in the ocean. To test the validity of these assumptions, we performed a binned statistical analysis on the GLAD data. This analysis showed a higher kinetic energy away from the boundaries, presumably a result of the loop current eddies (Figure S2).

The variance ellipses did not show any coherent patterns and suggested the flow variability is primarily isotropic. We repeated the analysis on smaller sections by dividing the data according to geographical region (Figures S3 and S4). The results from the more energetic regions indicated a slightly steeper $D2$ and $D2_r$ in the 5–50 km range, with the ratio $D2_t/D2_l$ peaking at 3. Also, the cross over of $D2_r$ and $D2_d$ happened at a smaller separation scale (~1 km; Figure S4).

To assess the extent to which inertial and super-inertial motions contribute to the structure functions, we repeated the analysis on frequency filtered Lagrangian velocity and position time series from the GLAD data (Figures S5 and S6). As Lagrangian measurements mix temporal and spatial information, filtering only in the frequency domain is not ideal. Also, it is not clear if the filtering should be performed only on the velocity time series or on both the velocity and position time series. This choice should mostly effect the results in the smaller separation bins, where the spatial resolution is finer, as the velocity difference samples are redistributed in separation bins due to filtering of the position time series. Due to these caveats, the results of the filtering should be viewed as suggestive rather than definitive. Removing only the inertial energy resulted in a small reduction of the divergent component below 10 km. However, it increased the contribution of the rotational component at length scales smaller than 5 km, which is likely a filtering artifact. Removing both the inertial and super-inertial energy led to a significant reduction in the divergent component below 10 km, a slight steepening of the rotational component in the 5–50 km range, aligning it more with the predictions for an enstrophy cascade, and a disappearance of the negative linear $D3_l$ ranges between 100 m and 2 km. These results suggest that the super inertial divergent motions might be strong contributors to the forward energy cascade and can also potentially contaminate the scaling behavior at the length scales of the enstrophy cascade. Choosing to only filter the velocity time series produced similar results (not shown).

5. Summary and Discussion

We have examined a Helmholtz decomposition of the second-order velocity structure function into rotational and divergent components, following [*Bühler et al.*, 2014; *Lindborg*, 2015], using velocities from surface drifters deployed in the GLAD experiment [*Poje et al.*, 2014]. This is the first such decomposition applied to Lagrangian data, and the smallest sampled scale, 10 m, is 2 orders of magnitude below that sampled in comparable ADCP studies [*Callies et al.*, 2014].

The results reveal that the rotational component dominates at scales above 5 km and the divergent component below. The Rossby number is approximately 1 at 1 km, so the divergent component emerges when Ro is order 1 or larger. The divergent component has a slope near 2/3 below 5 km, similar to an inertial energy range spectrum. The third-order velocity structure function is negative at these scales, implying a downscale cascade of energy.

The rotational velocity structure function has a steeper slope, roughly 1.5, from scales of 5 km up to the deformation radius. This is similar to a 2-D enstrophy cascade, although the slope is shallower than the predicted 2 for an inertial range of infinite extent. From L_d to 200 km, there is a brief 2/3 range, suggestive of a 2-D inverse energy cascade.

The results are reminiscent of those from the upper troposphere, where there is an enstrophy cascade from 2000 km down to several hundred kilometers and a transition to a shallower kinetic energy spectrum where $Ro \approx 1$ [*Nastrom and Gage*, 1985]. *Callies et al.* [2014] and *Callies et al.* [2016] used the MOZAIC (Measurement of OZone and water vapour by AIrbus in-service airCraft) data to show that the rotational energy spectrum dominates at the large scales near the tropopause, while the rotational and divergent components are nearly equal at the small scales. Structure functions, calculated with the same data, also show equal contributions at small scales, at least in the lower stratosphere, and a weaker divergent component in the upper troposphere across all scales [*Lindborg*, 2015].

In the present analysis, the rotational component is also greater at large scales, but the divergent component clearly dominates at small scales. A possible candidate for this large divergent contribution is inertial oscillations *Dewan* [1997], which are often significant in the ocean mixed layer and are prominent in the GLAD data [*Beron-Vera and LaCasce*, 2016]. Other candidates also exist, such as tidal motion [*Chavanne and Klein*, 2010] and wind forced surface flows, and have similar frequencies. However, it is difficult to test exactly which candidates dominate the divergent contribution with the present data set.

The second-order velocity structure function integrates across the energy spectrum and hence raises the question if the much greater divergent component seen in this study, when compared to the atmospheric literature, stems from the difference between spectra and structure functions. One can, in principle, calculate the spectra from the structure functions directly; however, this conversion is complicated by contributions from large scales, which are typically noisy with Lagrangian data (J. H. LaCasce, Calculating Energy Spectra from Drifters, submitted to *MDPI Fluids*), and does not produce meaningful results (not shown). Nevertheless, when the divergent spectrum is less than the rotational spectrum at large scales and equal at small scales, as in the atmospheric cases, the divergent structure function cannot exceed the rotational structure function. Thus, the present results imply that the divergent spectra actually do exceed the rotational spectra at small scales, again pointing to differences in the dynamics at smaller scales.

Studies in the Drake Passage and the Gulf Stream using ADCP data [*Bühler et al.*, 2014; *Callies and Ferrari*, 2013; *Rocha et al.*, 2015] observe a k^{-3} kinetic energy spectrum, transitioning to k^{-2} at smaller-length scales. A Helmholtz decomposition suggested roughly equal contributions from the divergent and rotational components at approximately 10 km in the Gulf Stream and 50 km in the Drake Passage. These studies show a wider range of scales over which a k^{-3} kinetic energy spectrum is observed, compared to the results presented here. The scales where the divergent components exceeded the rotational component were not resolved due to coarser resolution (1–5 km) of the ADCP data. *Bühler et al.* [2014] also show that in the eastern Subtropical North Pacific, which is less energetic than the Gulf Stream, the energy spectrum is closer to k^{-2} at all length scales smaller than 100 km, with no k^{-3} range.

Further work remains to be done, for instance, to illuminate the nature of the divergence-dominated regime and to test for seasonal variations [e.g., *Callies et al.*, 2015]. But the results of the present study shows that drifters can be used to deduce important aspects of the turbulent dynamics at lateral scales far below those sampled with most other instruments.

Acknowledgments
Geophysical Fluid Dynamics Institute contribution number 478. We thank Tamay Ozgokmen and the GLAD experiment team for making the data set available at https://data.gulfresearchinitiative.org/data/R1.x134.073:0004/, and Dr. Jörn Callies for bringing the method of Helmholtz decomposition for second-order velocity structure functions to our attention. D.B. and K.S. would like to acknowledge support from NSFOCE-1231803 and JHL to grant 221780 (NORSEE) from the Norwegian Research Council.

References

Babiano, A., C. Basdevant, and R. Sadourny (1985), Structure functions and dispersion laws in two-dimensional turbulence, *J. Atmos. Sci.*, *42*(9), 941–949, doi:10.1175/1520-0469(1985)042<0941:SFADLI>2.0.CO;2.

Bennett, A. (1984), Relative dispersion: Local and nonlocal dynamics, *J. Atmos. Sci.*, *41*(11), 1881–1886.

Beron-Vera, F. J., and J. H. LaCasce (2016), Statistics of simulated and observed pair separations in the gulf of Mexico, *J. Phys. Oceanogr.*, *46*, 2183–2199, doi:10.1175/JPO-D-15-0127.1.

Bühler, O., J. Callies, and R. Ferrari (2014), Wave-vortex decomposition of one-dimensional ship-track data, *J. Fluid Mech.*, *756*, 1007–1026, doi:10.1017/jfm.2014.488.

Callies, J., and R. Ferrari (2013), Interpreting energy and tracer spectra of upper-ocean turbulence in the submesoscale range (1–200 km), *J. Phys. Oceanogr.*, *43*(11), 2456–2474.

Callies, J., R. Ferrari, and O. Bühler (2014), Transition from geostrophic turbulence to inertia-gravity waves in the atmospheric energy spectrum, *Proc. Natl. Acad. Sci. U.S.A.*, *111*, 17,033–17,038.

Callies, J., R. Ferrari, J. M. Klymak, and J. Gula (2015), Seasonality in submesoscale turbulence, *Nat. Commun.*, *6*, 6862.

Callies, J., O. Bühler, and R. Ferrari (2016), The dynamics of mesoscale winds in the upper troposphere and lower stratosphere, *J. Atmos. Sci.*, doi:10.1175/JAS-D-16-0108.1.

Charney, J. G. (1971), Geostrophic turbulence, *J. Atmos. Sci.*, *28*(6), 1087–1095.

Chavanne, C. P., and P. Klein (2010), Can oceanic submesoscale processes be observed with satellite altimetry?, *Geophys. Res. Lett.*, *37*, L22602, doi:10.1029/2010GL045057.

Chelton, D. B., R. A. deSzoeke, M. G. Schlax, K. El Naggar, and N. Siwertz (1998), Geographical variability of the first baroclinic Rossby radius of deformation, *J. Phys. Oceanogr.*, *28*(3), 433–460, doi:10.1175/1520-0485(1998)028<0433:GVOTFB>2.0.CO;2.

Cho, J. Y., and E. Lindborg (2001), Horizontal velocity structure functions in the upper troposphere and lower stratosphere: 1. Observations, *J. Geophys. Res*, *106*, 10,223–10,232.

Davidson, P., and B. Pearson (2005), Identifying turbulent energy distributions in real, rather than Fourier, space, *Phys. Rev. Lett.*, *95*(21), 214501.

Davidson, P. A. (2015), *Turbulence: An Introduction for Scientists and Engineers*, Oxford Univ. Press, Oxford, U. K.

Dewan, E. (1997), Saturated-cascade similitude theory of gravity wave spectra, *J. Geophys. Res.*, *102*(D25), 29,799–29,817.

Frisch, U. (1995), *Turbulence: The Legacy of A. N. Kolmogorov*, Cambridge Univ. Press, Cambridge, U. K.

Gage, K. S., and G. D. Nastrom (1986), Spectrum of atmospheric vertical displacements and spectrum of conservative scalar passive additives due to quasi-horizontal atmospheric motions, *J. Geophys. Res.*, *91*(D12), 13,211–13,216, doi:10.1029/JD091iD12p13211.

Garrett, C., and W. Munk (1972), Space-time scales of internal waves, *Geophys. Astrophys. Fluid Dyn.*, *3*(1), 225–264.

Held, I. M., R. T. Pierrehumbert, S. T. Garner, and K. L. Swanson (1995), Surface quasi-geostrophic dynamics, *J. Fluid Mech.*, *282*, 1–20, doi:10.1017/S0022112095000012.

Kolmogorov, A. N. (1941), The local structure of turbulence in incompressible viscous fluid for very large Reynolds numbers, *Dokl. Akad. Nauk SSSR*, *30*, 301–305, JSTOR.

Kraichnan, R. H. (1967), Inertial ranges in two-dimensional turbulence, *Phys. Fluids*, *10*, 1417.

LaCasce, J. (2002), On turbulence and normal modes in a basin, *J. Mar. Res.*, *60*(3), 431–460.

LaCasce, J. (2008), Statistics from Lagrangian observations, *Prog. Oceanogr.*, *77*(1), 1–29.

LaCasce, J., and C. Ohlmann (2003), Relative dispersion at the surface of the gulf of Mexico, *J. Mar. Res.*, *61*(3), 285–312.

Le Traon, P.-Y., P. Klein, B. L. Hua, and G. Dibarboure (2008), Do altimeter wavenumber spectra agree with the interior or surface quasigeostrophic theory?, *J. Phys. Oceanogr.*, *38*(5), 1137–1142.
Lindborg, E. (1999), Can the atmospheric kinetic energy spectrum be explained by two-dimensional turbulence?, *J. Fluid Mech.*, *388*, 259–288.
Lindborg, E. (2006), The energy cascade in a strongly stratified fluid, *J. Fluid Mech.*, *550*, 207–242, doi:10.1017/S0022112005008128.
Lindborg, E. (2007), Horizontal wavenumber spectra of vertical vorticity and horizontal divergence in the upper troposphere and lower stratosphere, *J. Atmos. Sci.*, *64*(3), 1017–1025.
Lindborg, E. (2015), A helmholtz decomposition of structure functions and spectra calculated from aircraft data, *J. Fluid Mech.*, *762*, R4.
Lindborg, E., and J. Y. Cho (2001), Horizontal velocity structure functions in the upper troposphere and lower stratosphere. II—Theoretical considerations, *J. Geophys. Res.*, *106*, 10,233–10,241.
Morel, P., and M. Larceveque (1974), Relative dispersion of constant-level balloons in the 200-mb general circulation, *J. Atmos. Sci.*, *31*(8), 2189–2196.
Moum, J., and W. Smyth (2001), Upper ocean mixing processes, *Encyclopedia Ocean Sci.*, *6*, 3093–3100.
Nastrom, G., and K. S. Gage (1985), A climatology of atmospheric wavenumber spectra of wind and temperature observed by commercial aircraft, *J. Atmos. Sci.*, *42*(9), 950–960.
Pedlosky, J. (1987), *Geophysical Fluid Dynamics*, Springer, New York.
Poje, A. C., et al. (2014), Submesoscale dispersion in the vicinity of the deepwater horizon spill, *Proc. Natl. Acad. Sci. U.S.A.*, *111*(35), 12,693–12,698, doi:10.1073/pnas.1402452111.
Rocha, C. B., T. K. Chereskin, S. T. Gille, and D. Menemenlis (2015), Mesoscale to submesoscale wavenumber spectra in drake passage, *J. Phys. Oceanogr.*, *46*, 601–620, doi:10.1175/JPO-D-15-0087.1.
Rupolo, V., V. Artale, B. L. Hua, and A. Provenzale (1996), Lagrangian velocity spectra at 700 m in the western North Atlantic, *J. Phys. Oceanogr.*, *26*(8), 1591–1607, doi:10.1175/1520-0485(1996)026<1591:LVSAMI>2.0.CO;2.
Stammer, D. (1997), Global characteristics of ocean variability estimated from regional TOPEX/POSEIDON altimeter measurements, *J. Phys. Oceanogr.*, *27*(8), 1743–1769, doi:10.1175/1520-0485(1997)027<1743:GCOOVE>2.0.CO;2.
Thomas, L. N., A. Tandon, and A. Mahadevan (2008), Submesoscale processes and dynamics, in *Ocean Modeling in an Eddying Regime*, edited by M. W. Hecht and H. Hasumi, pp. 17–38, AGU, Washington, D. C.
Tulloch, R., and K. S. Smith (2006), A theory for the atmospheric energy spectrum: Depth-limited temperature anomalies at the tropopause, *Proc. Natl. Acad. Sci. U.S.A.*, *103*(40), 14,690–14,694, doi:10.1073/pnas.0605494103.
Wang, D.-P., C. N. Flagg, K. Donohue, and H. T. Rossby (2009), Wavenumber spectrum in the Gulf Stream from shipboard ADCP observations and comparison with altimetry measurements, *J. Phys. Oceanogr.*, *40*(4), 840–844, doi:10.1175/2009JPO4330.1.